



External Acoustical Damping on a Metallic Angle Wedge in a High Temperature Resistant Ultrasonic Probe

Oleg Shapovalov¹ · Thomas Heckel² · Mate Gaal² · Sabine Weiß¹

Received: 21 March 2022 / Accepted: 6 June 2022
© The Author(s) 2022

Abstract

Ultrasonic probes for high-temperature applications are provided with metallic wedges, which can withstand the contact with the high temperature of the inspected structure. The ultrasonic signal travels within the wedge and gets reflected from its boundaries, causing interference signals called “ghost echoes”. The current work presents an investigation of the additional damping effect provided by porous sintered metal plates applied onto the surface of the wedge. In particular, the study evaluates the effect of damping plate thickness on the interference signal level at different transmission frequencies. Damping plates made of sintered metal SIKA-R 15 AX were attached to a wedge prototype made of steel 1.4301. The study revealed, that the most effective thickness of damping plates in the selected frequency interval of 1 to 4 MHz is equal to 4 mm. The evaluation of the interference signal has shown that the application of such damping plates to the wedge surface contributes to an additional attenuation of an interference signal of 10 to 30 dB after 500 μ s of signal propagation.

Keywords Ultrasonic testing · High temperature · Acoustical damping · Angle wedge · Ultrasonic probe

1 Sound Absorption in an Ultrasonic Angle Beam Probe. External Wedge Damping

Non-destructive testing with ultrasound aims to measure and detect defects in parts by sending ultrasonic pulses into the material with subsequent evaluation of the received signals reflected in the workpiece. For optimal evaluation in many applications (e.g. to detect cracks perpendicular to the surface), the transmission pulse must be emitted at a non-normal angle into the workpiece surface [1]. The assembly of the angle beam probes used in such applications contains so-called angle wedges, which are usually made of thermoplastic resin. However, many industrial applications require ultrasonic measurement at elevated temperatures up to 500 °C [2], which does not allow the simple use of polymer components in the assembly of the measuring probes (the commercially available ultrasonic probes [15] for elevated temperatures use the wedge materials, which heat stability

normally doesn't exceed 200 °C). In these cases, the angle wedges are made of high-temperature resistant materials (e.g. stainless steel). Unfortunately, such a replacement of the wedge material often deteriorates the quality of the ultrasonic measurement due to the relatively low sound absorption of the temperature-resistant materials appropriate for use in wedge production [3, 4]. According to Eq. 1, this is a result of their high sound velocity:

$$\alpha = \frac{\omega^2}{2\rho C^3} \quad (1)$$

where α is the amplitude absorption coefficient, C is the longitudinal speed of sound, ρ is a density and cyclic frequency ω is equal to $2\pi f$ where f is the frequency of the wave [5]. The resulting low absorption of high-temperature resistant wedges leads to measurement disturbances (so-called “ghost echoes”) in the ultrasonic analysis due to internal reflection and propagation of the interfering signals within the wedge [6] (Fig. 1a. The elongated wedge designs [8] or delay lines [16, 17] can simultaneously provide the ghost echo weakening and passive cooling of transducer. As reported by [20], the ghost echos can be also eliminated by use of transmit-receiver probes. However, the reported designs lead to a crucial increase in transducer dimensions and production costs.

✉ Oleg Shapovalov
oleg.shapovalov@b-tu.de

¹ Brandenburg University of Technology (BTU)
Cottbus-Senftenberg, Cottbus, Germany

² Federal Institute for Materials Research and Testing (BAM),
Berlin, Germany

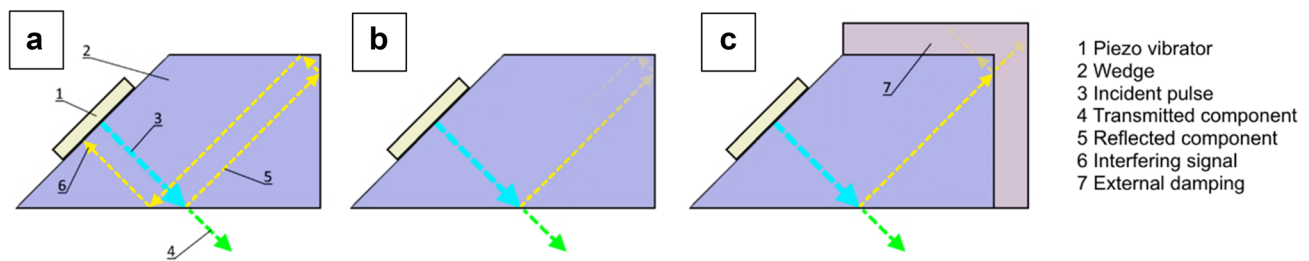


Fig. 1 Formation and propagation of an interfering signal inside the wedge of an angle beam ultrasonic probe: **a** wedge material with low sound absorption; **b** weakening of the interfering signal in the wedge material with high sound absorption; **c** weakening of the interfering signal in wedge material with low sound absorption using external damping

Besides the sound absorption, the interference signal can be also weakened by scattering (e.g. by means of fine dispersed inhomogeneities within the propagation medium) [7]. However, the high internal scattering inside the wedge would inevitably affect the transmitted signal as well (“4” in Fig. 1), and thus, reduce the sensibility of the probe. One of the common ways to avoid such impairment is an external damping [8] by means of attaching damping plates onto the surface of the wedge (Fig. 1c).

As reported in [18; 19] the porosity of solids has a positive effect on attenuation of ultrasonic waves propagating in material, which makes porous materials a promising solution for the external wedge damping. Furthermore, the coupling of the external damping to the wedge has to withstand thermal gradients, therefore the damping material has to suit the thermal expansion of the wedge. For this reason, the porous medium of a similar nature to a wedge would assure the most stable joining.

However, the porosity of a damping material shell not exceed extreme rates, because it inevitably decreases the acoustical impedance [14] of the material, thus decreasing the transmission into the external damping layer and eliminating the damping effectivity.

A 1991 patented construction of a high-temperature-resistant vertical ultrasonic transducer [11] utilizes the sinter-metallic “SIKA-R 15 AX” from GKN Sinter Metals Filters GmbH [9] as a backing body, showing a good backing performance at 2 MHz. Thanks to its porous structure (approx. 40% porosity with a pore size distribution of 13 to 30 μm), SIKA-R 15 AX may serve as a good scattering medium for ultrasonic waves [10]. On the other hand, made of steel 1.4404, it appears to be a perfect joining partner for the high-temperature stainless-steel wedge, being not only temperature resistant up to 540 $^{\circ}\text{C}$, but also able to withstand intensive heating and cooling rates as well. Based on these facts, it was decided to use the SIKA-R 15 AX as an external damping material for the high temperature-resistant steel wedge.

The current study aims to investigate the effectivity of described material as an external damping as well as to implement and test it on a steel wedge prototype.

2 Production of Laboratory Samples for the Normal Beam Testing

The first investigation step was to evaluate the general ability of the mentioned sintered material to dampen the ultrasonic signals in order to identify the most suitable thickness of the damping plates at normal incidence. Each laboratory sample produced for this purpose (see Fig. 2c) consists of a damping body (1) which is joined to a cylindrical front part (2) by means of brazing paste [12]. The tested damping bodies have a diameter of 20 mm and a thickness of 1, 2, 3, 6, 10, 15 and 21 mm, respectively. The front body has a length of 40 mm by the same diameter.

The parts to be joined were clamped together with a paste based on Ag 156 braze alloy on the joining surface and placed vertically in the furnace. A constant clamping force of 50 N was applied by means of a ceramic high-temperature resistant compression spring made of Si_3N_4 . The brazing process took place in a shielding gas furnace at a brazing temperature of 700 $^{\circ}\text{C}$ and a holding time of 30 min (see Fig. 2b). The preliminary holding at 200 $^{\circ}\text{C}$ for 30 min served to evaporate the flux residues before brazing. From 200 $^{\circ}\text{C}$ (when heating) and up to 400 $^{\circ}\text{C}$ (when cooling), the process took place in the inert gas atmosphere (argon sweep 300 l/min).

3 Damping Effect at Normal Incidence

The damping effect of the sintered metal at normal incidence was investigated at different frequencies, to determine the most effective thickness of the damping plates for each wavelength. For this purpose, a short longitudinal transmission pulse (frequencies 1, 2, and 4 MHz, piezo diameter 20 mm) was irradiated into the front body through an incident

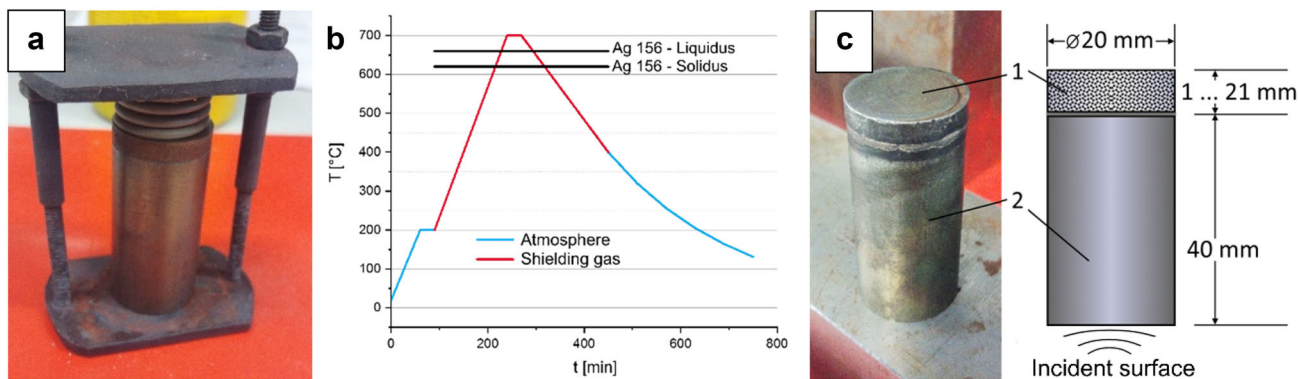


Fig. 2 Manufacturing of a laboratory sample to examine the damping ability at normal incidence: **a** clamping for brazing; **b** temperature–time diagram of the brazing process; **c** dimensions of the produced samples (exemplary in the photo-laboratory sample with 3 mm damping body)

surface on each of the prepared laboratory samples (Fig. 2c). The corresponding sound level was evaluated as follows:

$$L_{Dn} = 10 \lg(I_{Dn}/I_r), \tag{2}$$

with L_{Dn} is the evaluated received sound level of the respective laboratory sample with a damping body thickness of n mm, I_{Dn} is sound intensity of the received signal in the sample with a damping body thickness of n mm (see Fig. 3a). Since no absolute intensities were analyzed, the reference intensity I_r served only for an optimal representation and did not effect the evaluation results.

To investigate the effect of the damping material on direct backwall reflections, the intensity fall between the first and the second backwall echoes was calculated per wavelength for each sample and frequency and compared with the respective value of an "undamped" sample (without a damping body brazed on):

$$RDE_{Dn} = \Delta L_{Dn} - \Delta L_{D0} \tag{3}$$

with RDE_{Dn} is the reflection damping effect of a damping body with a thickness of n mm; ΔL_{Dn} and ΔL_{D0} are intensity falls between the first and the second backwall echoes.

An exemplary A-scan comparison and RDE calculation for 3 mm damping body at 4 MHz is shown in Fig. 3.

Due to a cylindrical form of a laboratory sample, besides the backwall echoes on the A-scan in Fig. 3, the repeating secondary echoes arising with constant delays of about $5.3 \mu s$ (at ca. $18.8, 24.1$ and $29.4 \mu s$ while the backwall echoes locate at 13.5 and $27 \mu s$). The mechanism of the formation of the secondary echos lies in the wave conversion on the side walls and is described in detail by [13].

The intensity fall between the backwall echoes as well as reflection damping effect depending on the thickness of the damping body and the transmission frequency are shown in the diagram in Fig. 4.

As can be seen from diagrams in Fig. 4, all the thicknesses of the damping body have a positive impact on the attenuation of the backwall echoes, however, no uniform pattern can be observed over different frequencies. While the RDE at 2 and 4 MHz increases with growing thickness up to approx. 0.25

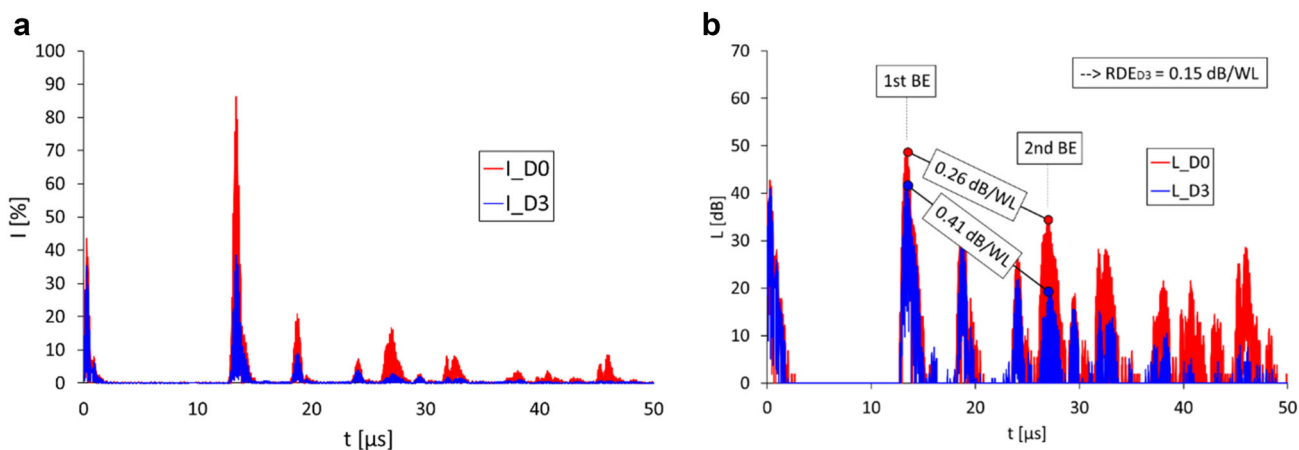


Fig. 3 Effect of a 3 mm damping body on the first echoes at normal incidence: **a** A-Scan; **b** respective calculation of a reflection damping effect

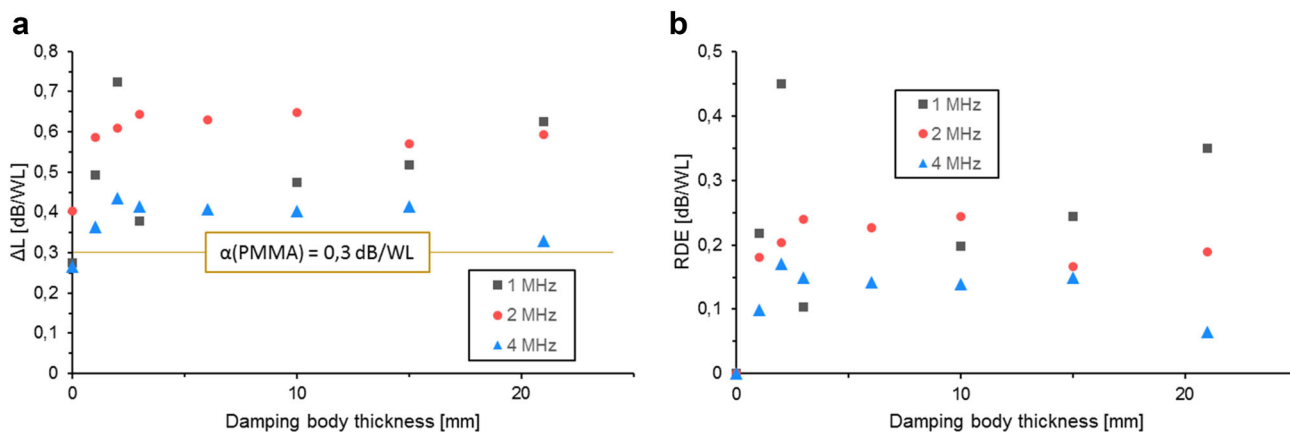


Fig. 4 Dependence of echo attenuation ΔL (a) and reflection damping effect RDE (b) on the thickness of the damping body at different transmission frequencies

and 0.15 dB per wavelength at 3 and 2 mm respectively, the damping effect at 1 MHz shows significant instability in the range up to 6 mm thickness followed by a continuous increase with a growing thickness.

The acoustic attenuation value of the PMMA (Plexiglas), measured by [21], is given in Fig. 4, a only as a benchmark, since it may not include some local experimental factors such as e.g. echo attenuation due to mode conversion on the side walls of cylindrical laboratory sample or transmission losses into the ultrasonic transducer. Moreover, the observed significant attenuation of direct reflections is a result of the signal scattering and may allegedly have a lower effect on noise attenuation on higher time of flight ranges. The reason for this is that the scattering, effectively suppressing the single echoes, may have a much smaller impact on more homogeneous noise level observed at higher time of flight.

To quantify the damping effect on a noise level on higher time of flight ranges, the averaged signal level curves L_{avg} were calculated for each sample and frequency up to 500 μs . An example of the evaluation of the damping effect (“DE”) for a 3 mm thick damping body at signal frequency 4 MHz is represented in the diagram in Fig. 5.

Each curve in Fig. 5 depicts a moving average (averaging interval $\pm 10 \mu\text{s}$) of the corresponding sound level curve. To determine the overall damping effect DE, the curves were linearized in the range from 300 to 500 μs , so that the end of each line is taken as the final height $L_{Dn}(500)$. The difference between this value and the corresponding value of the “undamped” sound level $L_{D0}(500)$ is considered to be the damping effect DE_{Dn} of the respective damping body thickness at the selected frequency (see formula 4).

$$DE_{Dn} = L_{\text{avg}_D0}(500) - L_{\text{avg}_Dn}(500) \quad (4)$$

The damping effect depending on the thickness of the damping body and the transmission frequency is shown in the diagram in Fig. 6.

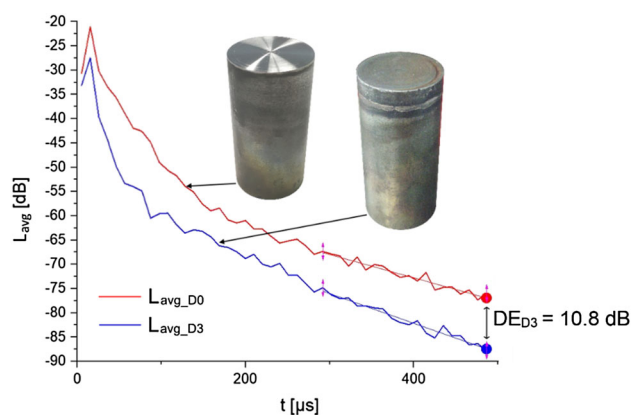


Fig. 5 Exemplary evaluation of the damping effect DE for a damping body with 3 mm thickness

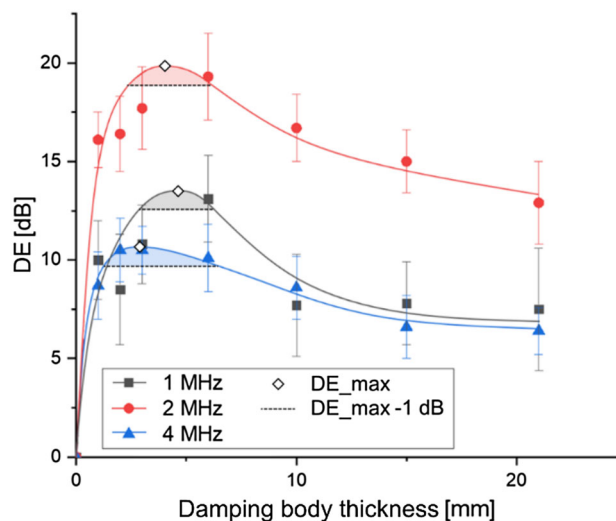


Fig. 6 Dependence of the damping effect DE on the thickness of the damping body at different transmission frequencies (points—measurement results; lines—estimated course)

The diagram in Fig. 6 clearly shows that the selected sinter-metallic material "SIKA-R 15 AX" has different damping effects at different frequencies, where the highest damping effect occurs at a signal frequency of 2 MHz. The estimated damping effect at this frequency is up to approx. 19.8 dB, while 1 MHz and 4 MHz signals could only be attenuated by a maximum of 13.5 and 10.6 dB, respectively.

Since the total attenuation of an ultrasonic signal includes scattering in addition to material absorption, which, according to Eq. 1, increases with increasing frequency, this could theoretically explain the lower damping of the 1 MHz signal. However, since the values depicted in Fig. 6 are calculated as the difference from the attenuation in the "undamped" specimen (see Fig. 5), in which the corresponding absorption of the stainless steel after 500 μ s of propagation is already included, it can be concluded, that the observed dependence (Fig. 6) is due to differences in scattering.

With a purpose to evaluate the scattering behavior at different frequencies, the respective wavelengths were defined and weighed with the structure of the sintered material. Due to the strong scattering of the material, the precise measurement of its longitudinal speed of sound was complicated and revealed only approximate values of about 2000 m/s, which results in wavelength evaluation of approx. 2000, 1000, and 500 μ m for 1, 2, and 4 MHz signals respectively.

Although the pore size of damping material was given as 13...30 μ m, the metallographic study (Fig. 7) has shown, that along the fine pores under 100 μ m, there are many larger irregularities (marked in yellow) in the pore distribution which have the comparable size with the evaluated wavelengths.

Thus, it can be assumed, that the inhomogeneities present in the used material are too coarse for a shorter wavelength

(4 MHz signal frequency), so that the individual pores act as relatively large reflective surfaces (schematic in Fig. 8a) being unable to provide optimal scattering. However, in the case of a 1 MHz signal, the wavelength is so large relative to the pore size that the wave can propagate through such a fine-grained structure with relatively little attenuation (Fig. 8c).

Therefore, for an optimum damping effect, the suitable pore size of a damping material has to be adjusted separately for each frequency.

Contrary to the assumption that the increasing thickness of a damping body would continuously lead to an increase in the damping effect, the diagram in Fig. 6 shows that the damping effect increases at all frequencies only up to a certain thickness, followed by a slower decrease afterward. This can be explained by the return of the wave components from the damping body, which then interfere with the remaining signal components propagating in the forward body. Thus, the specific damping body thickness can lead to a favorable interference pattern, if the wave interference results in additional weakening of the interference signal. The diagram in Fig. 6 shows which thickness ranges of the damping body can be considered suitable for the different transmission frequencies. If we define the suitability criterion so that damping effect is at the most 1 dB lower than the maximum damping (dashed lines in Fig. 6), the suitable thickness ranges are as follows:

- 2,9 to 6,4 mm for 1 MHz ($DE_{max} \sim 13,5$ dB at approx. 5 mm)
- 2,4 to 6,2 mm for 2 MHz ($DE_{max} \sim 19,8$ dB at approx. 4 mm)
- 2,4 to 6,3 mm for 4 MHz ($DE_{max} \sim 10,6$ dB at approx. 3 mm)

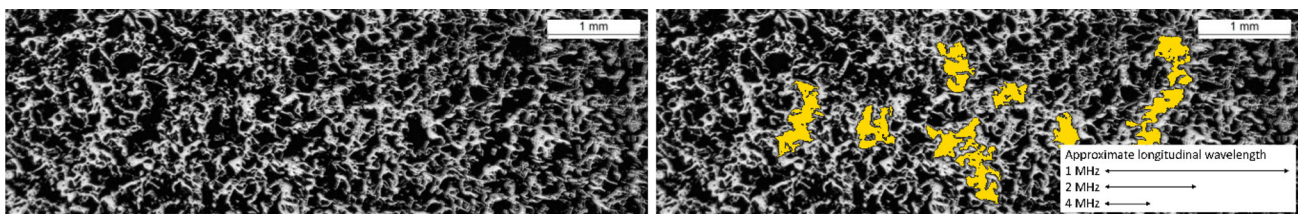


Fig. 7 Metallographic study of the damping material

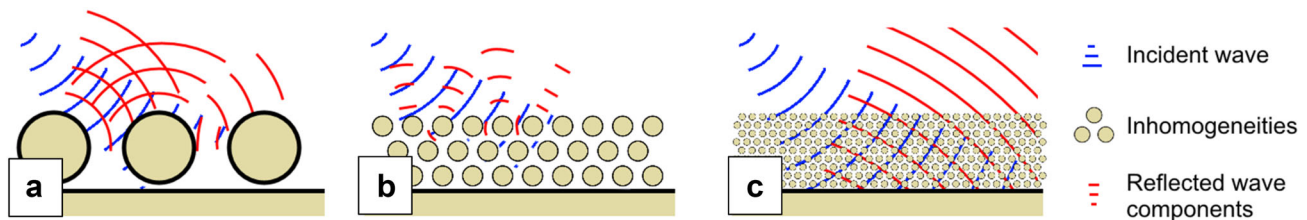


Fig. 8 Scattering Effectivity of the sound waves depending on the size of the inhomogeneities in the damping layer (a damping material too coarse; b suitable damping material; c damping material too fine)

4 Damping Effect on the Metallic Wedge Prototype

The next step was to verify and evaluate the effectiveness of the sintered metal cover plates as external acoustic damping on a wedge body.

For this purpose, a prototype of the high-temperature-resistant ultrasonic wedge made of stainless steel 1.4301 (Fig. 9a; wedge width 20 mm) was provided with damping plates on all surfaces except for the incident and transmission ones (see Fig. 9a).

In contrast to a normal incidence, the waves in the wedge transmit into the damping plates under different angles, producing in addition shear components (see Fig. 10). However,

due to the velocity differences between the wedge and damping material (for approx. longitudinal sound velocity in the damping material, see chapter 3), the transmitting angles are significantly lower than the incident ones (see Fig. 10).

Thus, the first wave incidents into the damping plates, which allegedly contribute the significant impact on the overall scattering, will produce the waves at following angles:

$$\theta_{RS1} = \arcsin\left(\frac{C_{WT}}{C_{WL}} \cdot \sin(\theta_{IP1})\right) = 23.3 \quad (5)$$

$$\theta_{RP1} = \theta_{RP1} = 45 \quad (6)$$

$$\theta_{IS2} = \theta_{RS1} = 23.3 \quad (7)$$

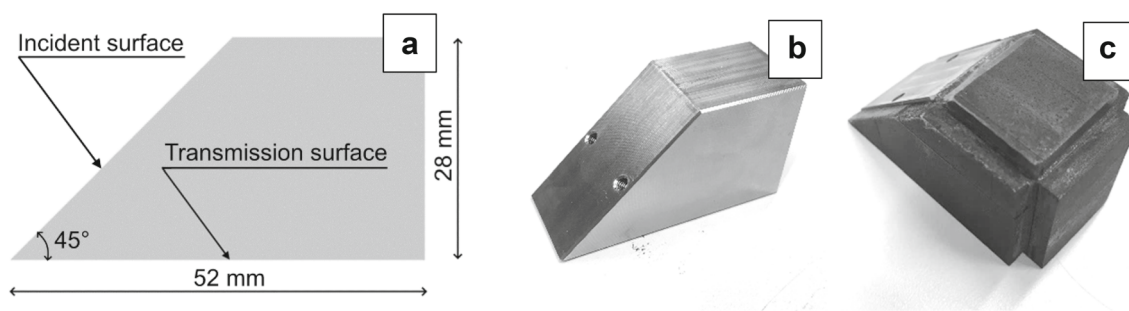


Fig. 9 Prototype of a high temperature resistant ultrasonic wedge: **a** wedge dimensions; **b** photo of a wedge without external damping; **c** photo of the wedge with damping plates

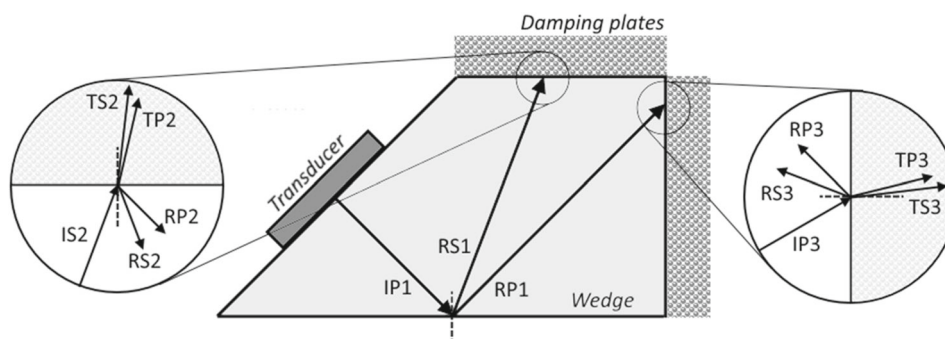


Fig. 10 First wave interactions at the damped surfaces in the wedge prototype

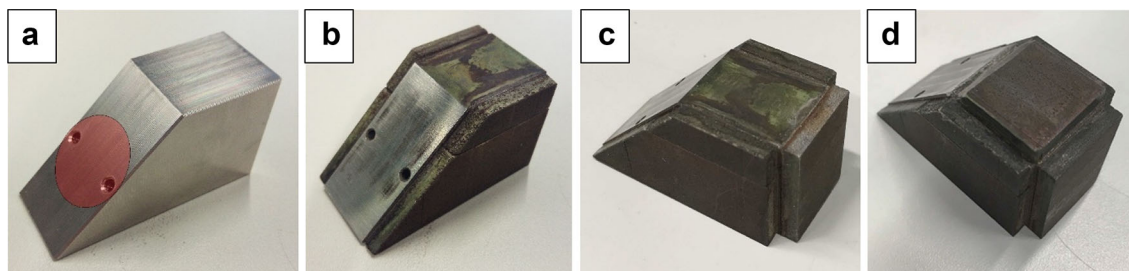


Fig. 11 Step-by-step attachment of the damping plates: **a** wedge prototype without damping (placing area for the transducer – in red); **b** laterally damped wedge prototype; **c** laterally and frontally damped wedge prototype; **d** fully damped wedge prototype (lateral, frontal and on the top)

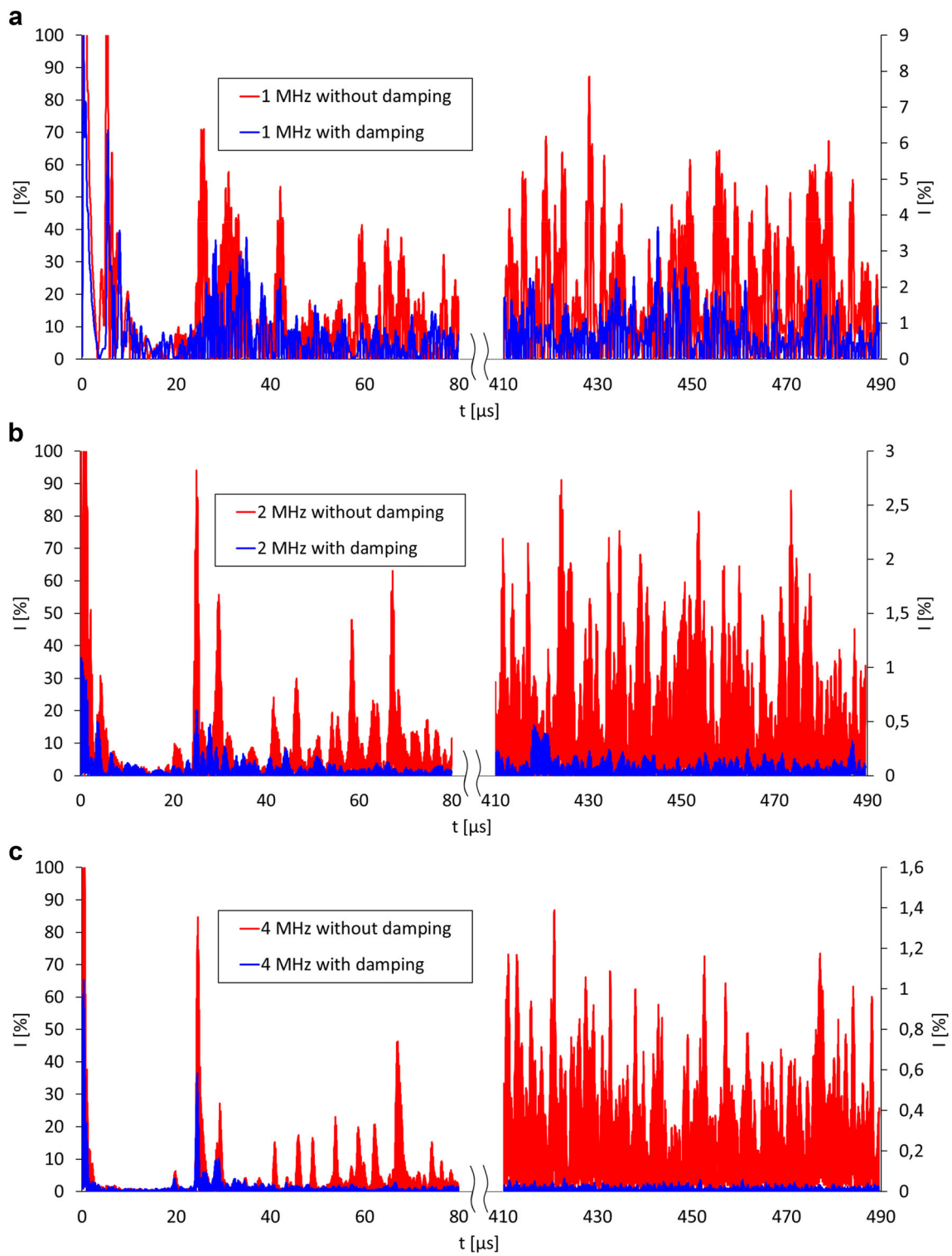


Fig. 12 Damping effect of the sintermetallic plates (all sides damped) on the signal propagating in the wedge at 1 (a), 2 (b) and 4 MHz (c)

$$\theta_{IP3} = 90^\circ - \theta_{RP1} = 45 \tag{8} \quad \theta_{TP2} = \arcsin\left(\frac{C_{DL}}{C_{WT}} \cdot \sin(\theta_{IS2})\right) = 13.6^\circ = \theta_{TP3} \tag{10}$$

$$\theta_{TS2} = \arcsin\left(\frac{C_{DT}}{C_{WT}} \cdot \sin(\theta_{IS2})\right) = 7.4^\circ = \theta_{TS3} \tag{9}$$

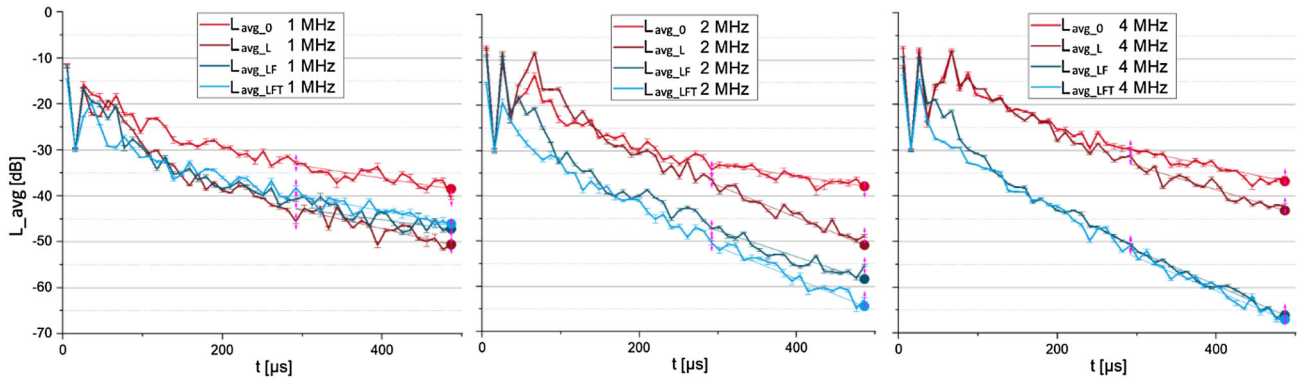


Fig. 13 Received signal level after different steps of attaching the damping plates to the wedge prototype

Table 1 Effect of attaching the damping plates on different wedge surfaces on the interference signal level after 500 μs propagation

	1 MHz	2 MHz	4 MHz
DE _L	12.1 dB	13.0 dB	6.4 dB
DE _F	− 3.4 dB	7.5 dB	22.9 dB
DE _T	− 0.9 dB	6.0 dB	1.0 dB
DE _{LFT}	7.8 dB	26.5 dB	30.3 dB

with θ are the angles of incidence, transmission and reflection (“I”, “T” and “R” as the first index respectively) of plane and shear waves (“P” and “S” as the second index); C_{WL} and C_{WT} are longitudinal and transversal velocities in the wedge; as well as C_{DL} and C_{DT} are these for the damping material respectively.

Therefore, at least the first transmissions shown in Fig. 10 propagate in the damping material at the angle of $13,6^\circ$ for longitudinal transmission, which makes their time of flight in the damping plate only approx. 3% longer then by a normal incidence ($\cos^{-1}(13,6^\circ) = 1,03$). Thus, based on the investigation of the thickness dependence of the damping effect (see Chapter 3), the 4 mm thickness, described as a best suitable for a normal incidence, has been implemented in the prototype damping as well.

The investigation of the damping effect on the wedge prototype is analogous to the normal sound incidence described in chapter 3. The incidence was transferred to a wedge with the same probes (1, 2 and 4 MHz, piezo diameter 20 mm) in the center of the surface of the wedge (red in Fig. 11a).

Since placing the damping plates on different wedge surfaces can contribute differently to the resulting damping effect, the damping plates were placed step by step (Fig. 11, brazing process analogous to Chapter 3) and the sound level was measured each time, to evaluate the individual damping effects of each surface.

The A-scans showing the effect of the damping plates on ghost echoes in the wedge as well as on the noise level at

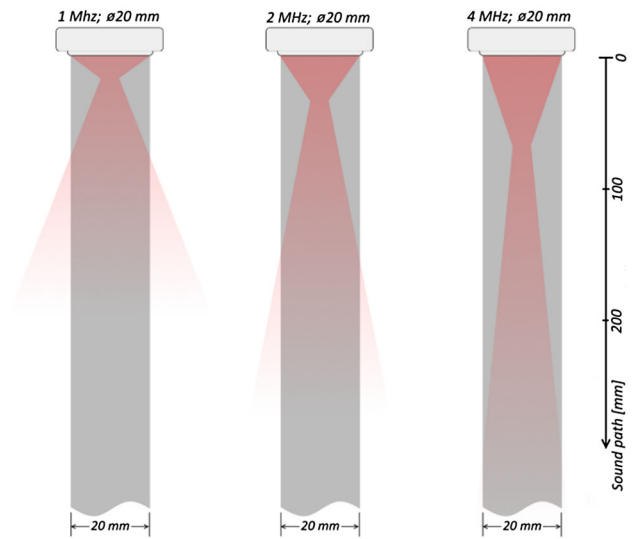


Fig. 14 Schematic comparison of a “− 20 dB” sound beam spread of different frequencies in stainless steel related to the specified wedge width of 20 mm (speed of sound 6010 m/s [13])

higher time of flight by different frequencies can be observed in Fig. 12.

As can be seen in Fig. 12, at all of the studied frequencies the damping plates have a noticeable effect both on the ghost echoes at shorter time of flight and on the noise attenuation at higher time of flight ranges. However, the most effective damping can be observed at 2 and 4 MHz.

The effect of the damping of each wedge surface at 500 μs of the respective wedge surface using aberaged sound level curves was calculated as follows:

$$DE_L = L_{avg_0}(500) - L_{avg_L}(500) \tag{11}$$

$$DE_F = L_{avg_L}(500) - L_{avg_LF}(500) \tag{12}$$

$$DE_T = L_{avg_LF}(500) - L_{avg_LFT}(500) \tag{13}$$

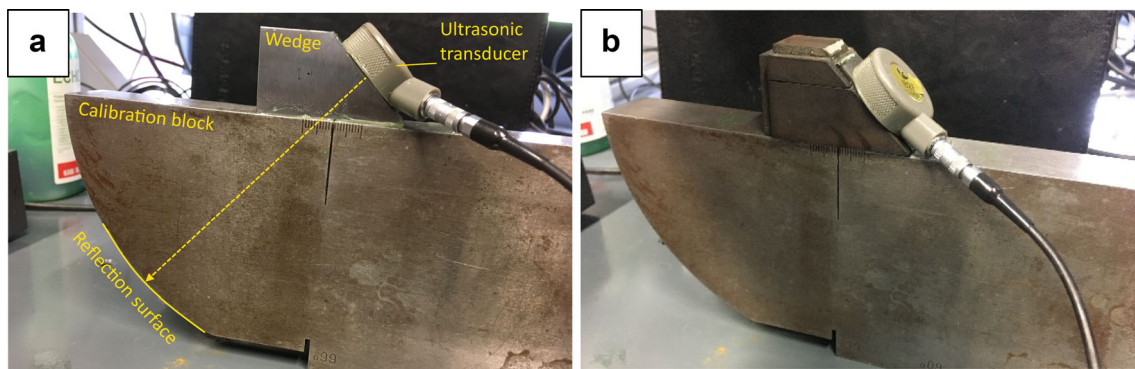


Fig. 15 Experimental setup for evaluation of the damping effect on the signal noise ratio (**a** wedge without damping; **b** damped wedge)

$$DE_{LFT} = L_{avg_0}(500) - L_{avg_LFT}(500) \quad (14)$$

where $L_{avg_0}(500)$, $L_{avg_L}(500)$, $L_{avg_LF}(500)$ and $L_{avg_LFT}(500)$ are the averaged received signal levels after 500 μ s propagation in the respectively dampened wedge prototype (see Fig. 13 a, b, c and d respectively); while DE_L , DE_F , DE_T and DE_{LFT} are the effects of the lateral, frontal and top damping, respectively.

The sound level curves as well as the resulting damping effects calculated at different frequencies are shown in the diagrams in Fig. 13 and listed in Table. 1.

According to Table. 1 and the diagrams in Fig. 13, at lower frequencies, lateral damping is more important, while frontal damping gains importance at 4 MHz. The obvious reason is the different spread of the sound beam at different frequencies (see Fig. 14).

Since the sound beam opening angle decreases with increasing frequency, most of the sound energy of the high-frequency signal falls on the front and top of the wedge, which means that the frontal and top damping is more effective. Lateral damping is most effective for the wider 1 MHz sound beam since the propagating ultrasonic signal reaches the lateral wedge surfaces very quickly and with a relatively high sound pressure. According to Table. 1, the effect of the upper and frontal attenuation on the total descent of a 1 MHz signal even results in negative values. This is probably the consequence of the stepwise brazing process: the already existing brazing layers on the wedge sides were remelted during the subsequent brazing steps, which could worsen the effect of the lateral damping due to the deterioration of the remelted joint quality.

With a purpose to estimate the effect of the damping plates on a signal-to-noise ratio, the wedge prototype was coupled to the calibration block (see Fig. 15).

Comparative A-scans of respective backwall signal detection at different frequencies are shown in Fig. 16.

As can be seen from Fig. 16, the damping plates, in addition to the suppression of ghost echoes, increase the echo height of the main signal as well as decrease the noise level. The evaluation of the respective SNR is represented in Table. 1.

5 Conclusions

In the present study, the ability of sintered metal material to attenuate the ultrasonic interference signals in a temperature-resistant stainless steel ultrasonic wedge from the outside was investigated. The described method seems to be an effective solution to reduce the interference signals propagating in the wedge. Therefore, the described external damping technique can significantly improve the measurement quality in high-temperature-resistant ultrasonic probes.

The investigation of the damping of ultrasonic signals at normal incidence has shown that the sintered metal layers with the thicknesses from 3 to 5 mm brazed on the surface of a metal body can cause a significant weakening of the propagating ultrasonic signal for the frequency range from 1 to 4 MHz. In addition, the measurements show that the selected damping material most effectively affects the propagation of the 2 MHz signal. At lower and higher frequencies, adjusting the grain size and porosity of the damping material can provide more effective external ultrasonic damping.

Implementation of the investigated damping technique on an industrial high temperature resistant stainless steel wedge prototype has shown that attaching the 4 mm thick damping plates to the surfaces of the prototype can reduce the level of the interfering “ghost signals” propagating in the wedge by up to 30 dB after 500 μ s time of flight. In addition, the investigation showed that at low frequencies attaching the damping plates to the side surfaces of the wedge is most effective, while for a high-frequency signal damping the front of the wedge is more important.

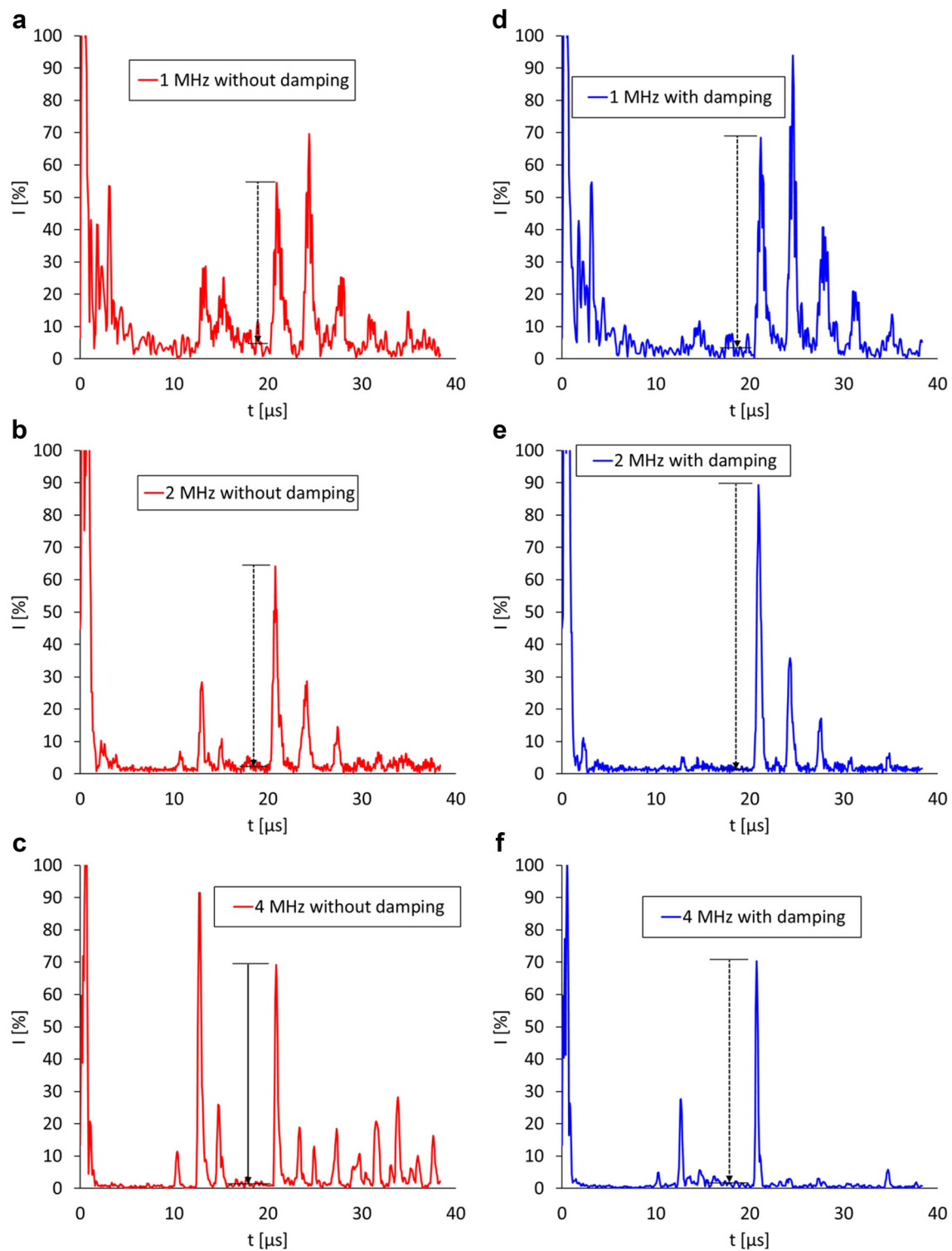


Fig. 16 Evaluation of a backwall reflection on the calibration block using the wedge without (**a**, **b** and **c** for 1, 2 and 4 MHz respectively) and with the external damping (**d**, **e** and **f** for 1, 2, and 4 MHz respectively)

However, in short time of flight range, especially for 4 MHz, the damping plates have the most impact on the suppression of ghost echoes rather than on the noise level (see

Fig. 16 and Table. 2). The reason is that the noise reduction by use of the external damping has a cumulative effect, becoming more noticeable with increasing time of flight (Fig. 12),

Table 2 Evaluation of a signal-to-noise ratio of the test on the calibration block

	1 MHz		2 MHz		4 MHz	
	Without damping	With damping	Without damping	With damping	Without damping	With damping
Signal [%]	54.5	68.5	64.2	89.3	69.2	70.4
Noise [%]	4.6	2.3	1.9	1.5	1.5	1.5
SNR [dB]	21.5	29.5	30.6	35.5	33.3	33.4

which can be very useful, particularly in ultrasonic flow measurement.

Funding Open Access funding enabled and organized by Projekt DEAL. This study was carried out as a part of a ZIM-Project (Central Innovation Programme for SMEs) in cooperation with the industrial partner FLEXIM Flexible Industriemesstechnik GmbH and received a financial support from the German Federation of Industrial Research Associations (AiF) under the Grant Number ZF4044212JA7.

Declarations

Conflict of interest The authors declare that they have no known competing financial interests or personal relationships that could have appeared to influence the work reported in this paper.

Open Access This article is licensed under a Creative Commons Attribution 4.0 International License, which permits use, sharing, adaptation, distribution and reproduction in any medium or format, as long as you give appropriate credit to the original author(s) and the source, provide a link to the Creative Commons licence, and indicate if changes were made. The images or other third party material in this article are included in the article's Creative Commons licence, unless indicated otherwise in a credit line to the material. If material is not included in the article's Creative Commons licence and your intended use is not permitted by statutory regulation or exceeds the permitted use, you will need to obtain permission directly from the copyright holder. To view a copy of this licence, visit <http://creativecommons.org/licenses/by/4.0/>.

References

1. The International Atomic Energy Agency. Ultrasonic Testing of Materials at Level 2g. IAEA-TECDOC-462. Vienna, Austria (1988)
2. Atkinson, I., Gregory, C., Kelly, SP., Kirk, KK. Ultrasmart: developments in ultrasonic flaw detection and monitoring for high-temperature plant applications. Proc. CREEP8. <https://doi.org/10.1115/CREEP2007-26411> (2007)
3. Shapovalov, O., Gaal, M., Hönig, G., Gradt, T., Weiß, S. Temperature dependence of the propagation speed of a longitudinal wave in different solids for use as a wedge material in an extreme temperature-resistant ultrasonic transducer. Proc. 23rd ICA: 4758. <https://doi.org/10.18154/RWTH-CONV-239953> (2019)
4. Grellmann, W., Seidler, S.: Zerstörungsfreie Kunststoffprüfung, 3rd edn., pp. 461–528. Carl Hanser Verlag, München (2015)
5. Kostyuk, D.A., Kuzavko, Yu.A.: Anomalies in the Ultrasound Reflection from a Solid-Dissipative Medium Interface. Tech. Phys. Lett. **27**(12), 994 (2001). <https://doi.org/10.1134/1.1432326>
6. Matthies, K.: Dickenmessung mit Ultraschall, 2nd edn. DVS Media Verlag, Berlin (1998)
7. Meschede, D.: Gerthsen Physik. Springer-Verlag, Berlin (2015)
8. Marvasti, M., Bond, J., Matheson, M., Sinclair, A.N.: Phased array inspection at elevated temperatures: effects of ultrasonic beam skew. Insight **56**(5), 257 (2014). <https://doi.org/10.1784/insi.2014.56.5.256>
9. SIKAR... AX“ Brochure. GKN Sinter Metals Filters GmbH. <https://www.gknp.com/globalassets/downloads/powder-metallurgy/2017/sika-r-ax-english.pdf>
10. Deutsch, M., Platte, V., Vogt, M.: Ultraschallprüfung. Grundlagen und industrielle Anwendungen. Springer, Berlin (1997)
11. Bärsch, W., Blasius, D., Kanngiesser, P., Podgorski, J., Matthies, K., Mrasek, H., Beyer, R. Patent EP0459431A2: Ultrasonic measuring probe for hot environments (1990)
12. Brazing - Filler metals. DIN EN ISO 17672:2010–11
13. Krautkrämer, J., Krautkrämer, H.: Metallische Werkstoffe und ihre besonderen Prüfaufgaben, pp. 312–531. Springer, Berlin (1980)
14. Mahbaz, B., Memarian, H. Lithology Prediction of Fahliyan Formation Based on Rock Physics Studies in Two Wells of Two Neighbor Oil Fields, Southwest of Iran. 5th Asian Rock Mechanics Symposium (ARMS5), p 389 (2008)
15. <https://www.olympus-ims.com/en/applications/ultrasonic-phased-array-wedge-for-inspecting-high-temperature-parts-up-to-150c/>
16. Kazys, R.: Vaskeliene V (2021) high temperature ultrasonic transducers: a review. Sensors **21**(3200), 3 (2021). <https://doi.org/10.3390/s21093200>
17. <https://www.olympus-ims.com/data/File/panametrics/panametrics-UT.en.pdf>
18. Sarpüna, H., Özkanb, V., Yönetkenc, A., Erolc, A.: Mean grain size and pore effects on ultrasonic properties of WC-Fe-Ni and SiC-Fe-Ni composites. Acta Phys. Pol. A **123**, 691 (2013). <https://doi.org/10.12693/APhysPolA.123.688>
19. Duitama-Leal, A., Almanza, O., Montes-Vides, L.: Modeling attenuation and dispersion of acoustic waves in porousmedia containing immiscible non viscous fluids. Dyna **83**(199), 81 (2016). <https://doi.org/10.15446/dyna.v83n199.56238>
20. Kumar, S., Menaka, M., Venkatraman, B.: Simulation and experimental analysis of austenitic stainless steel weld joints using ultrasonic phased array. Meas. Sci. Technol. **31**, 024005 (2020). <https://doi.org/10.1088/1361-6501/ab48a3>
21. Bloomfield, P.E., Lo, W.J., Levin, P.A.: Experimental study of the acoustical properties of polymers utilized to construct PVDF ultrasonic transducers and the acousto-electric properties of PVDF and P(VDF/TrFE) films. IEEE Trans. Ultrason. Ferroelectr. Freq. Control **47**(6), 1398 (2000). <https://doi.org/10.1109/58.883528>

Publisher's Note Springer Nature remains neutral with regard to jurisdictional claims in published maps and institutional affiliations.